Measurement of the Jet Transverse Momentum Resolution and Searches for New Physics in Events with Jets and Missing Transverse Momentum at the CMS Experiment

Dissertation

zur Erlangung des Doktorgrades

des Fachbereichs Physik

der Universität Hamburg

vorgelegt von

Kristin Goebel geb. Heine

aus Gifhorn

Hamburg

2014

Gutachter der Dissertation:	Prof. Dr. bla Prof. Dr. bla
Gutachter der Disputation:	Prof. Dr. bla Prof. Dr. bla
Datum der Disputation:	??. ?? 2014
Vorsitzender des Prüfungsausschusses:	Dr. bla
Vorsitzender des Promotionsausschusses:	Prof. Dr. bla
Leiterin des Fachbereichs Physik:	Prof. Dr. bla
Dekan der Fakultät für Mathematik, Informatik und Naturwissenschaften:	Prof. Dr. bla

Abstract

The search for signals of new physics processes beyond the standard model of particle physics is one of the main goals of the CMS experiment at the CERN Large Hadron Collider. Since many theories like e.g. supersymmetry involve the production of new coloured particles which feature jets as their experimental signature, it is important to have a good understanding of jet properties in order to allow such searches.

In the first part of this thesis, a measurement of the jet transverse momentum resolution is presented based on the analysis of proton-proton collision data recorded at a center of mass energy of 8 TeV by the CMS experiment. The measurement utilizes the transverse momentum balance of dijet events at particle level. The main focus lies on the determination of the data-to-simulation ratio of the resolution which can be used to derive scale factors in order to correct the resolution in simulated events to match the observed resolution in data.

The second part of the thesis focuses on searches for supersymmetry in final states with jets and missing transverse momentum. First, a search performed on collision data recorded at $\sqrt{s} = 8$ TeV is presented which targets mainly signatures sensitive to the production of light squarks and gluinos as well as the production of gluino mediated third generation particles. Here the main focus lies on the estimation of background contributions arising from QCD multijet events. Second, a study based on simulated events at a center of mass energy of 13 TeV is shown investigating different search strategies towards the identification of directly produced top squarks. Utilizing algorithms for the identification of boosted hadronically decaying top quarks arising from the decay of heavy top squarks, a search sensitivity of top squark masses up to 1 TeV is expected for LSP masses less than approximately 200 GeV.

Kurzfassung

Die Suche nach Hinweisen auf Prozesse von neuer Physik jenseits des Standardmodells der Teilchenphysik ist eines der Hauptziele des CMS Experiments am CERN Large Hadron Collider. Da zahlreiche Theorien wie beispielsweise Supersymmetrie die Produktion von neuen farbgeladenen Teilchen, welche als experimentelle Signatur Jets aufweisen, beinhalten, ist es wichtig ein gutes Verständnis dieser Objekte zu erlangen um derartige Suchen zu ermoeglichen.

Im ersten Teil dieser Arbeit wird eine Messung der Jet-Transversalimpuls-Auflösung vorgestellt, welche auf der Analyse von Proton-Proton-Kollisionsdaten basiert, die bei einer Schwerpunktsenergie von 8 TeV vom CMS Experiment aufgezeichnet wurden. Die Messung nutzt dabei die Transversalimpulsbalance von Zweijet-Ereignissen auf Teilchenniveau. Der Fokus liegt dabei auf der Bestimmung des Verhältnisses der Auflösung in Daten zu der Auflösung in simulierten Ereignissen, welches verwendet werden kann um Skalierungsfaktoren zu bestimmen, welche die in simulierten Ereignissen gemessene Auflösung an die in Daten beobachtete anpassen.

Der zweite Teil der Arbeit konzentriert sich auf Suchen nach Supersymmetrie in Endzuständen mit Jets und fehelndem Transversalimpuls. Zunächst wird eine Suche unter Verwendung von bei einer Schwerpunktsenergie von $\sqrt{s} = 8$ TeV aufgezeichneten Kollisionsdaten durchgeführt, die auf Signaturen abzielt, welche hauptsächlich sensitiv sind auf die Produktion von leichten Squarks und Gluinos sowie die Produktion von gluinoindizierten Teilchen der dritten Generation. Der Schwerpunkt liegt hier auf der Abschätzung des Untergrundbeitrags durch QCD Mulijet Ereignisse. Als zweites wird eine Studie vorgestellt, welche auf simulierten Ereignissen bei einer Schwerpunktsenergie von 13 TeV basiert und unterschiedliche Analysestrategien zur Identifikation von direkt produzierten Top Squarks untersucht. Unter Verwendung von Algorithmen zur Identifikation von geboosteten hadronisch zerfallenden Top Quarks aus den Zerfällen von Top Squarks, kann eine Sensitivität der Suche für Top Squarks Massen bis 1 TeV für LSP Massen bis circa 200 GeV erwartet werden.

Contents

1 Introduction

The current knowledge and understanding of the fundamental constituents of matter and occuring interactions between them are summarized in the well-established standard model (SM) of particle physics. The SM which has been introduced in the early 1970's is to date a very successful theory as it was able to predict new particles in the past and is tested to very high precision. Beyond that there are several other fundamental questions unanswered like the origin of dark matter or the unification of coupling constants at a certain scale. One of such theories which goes beyond the standard model and is supposed to provide a solution to such open problems is *supersymmetry* (SUSY). A short introduction to the phenomenology of the standard model as well as supersymmetry can be found in Chapter 1 of this thesis.

In order to address all such questions about tests of the SM and new theories beyond, the CMS experiment located at the Large Hadron Collider (LHC) at CERN [1] has been build. It is designed to analyse particle collisions delivered by the LHC and is the experiment in whichs context this thesis has been performed. An overview of the technical setup of the CMS experiment as well as the current status of its' operation is given in Chapter 2. The general introduction to the CMS experiment is followed in Chapter 3 by an introduction to the reconstruction of certain objects recorded in the particle collisions as well as dedicated algorithms to identify specific decay processes, like e.g. decays of top-quarks.

As the name already indicates, the LHC is a hadron collider and thus the predominant objects to be measured in the detector are expected to be jets – the experimental signature of quarks and gluons. Thus it is very important to have a good understanding of these objects as e.g. a precise knowledge of the jet transverse momentum resolution. A measurement of this quantity in data recorded by the CMS experiment at a center-of-mass energy of 8 TeV as well as simulated events is a main topic of this thesis and discussed in detail in Chapter 4.

The detailled knowledge about jets and their resolution can afterwards be exploited in a search for new physics mainly targeting signatures of decays involving supersymmetric particles in events with missing transverse energy and several jets. The main subject of this thesis is here the estimation of background contributions arising from mismeaured jets and the decay of heavy flavour quarks to the decays of interest. An overview of this analysis with special emphasis on the QCD multijet background determination is presented in Chapter 5.

Finally, Chapter 6 summarizes a prospect study for searches for supersymmetry at a center-of-mass energy of 13 TeV which will be most likely the operation energy of the LHC in 2015 when the operation is restartet. The thesis ends with a short summary and outlook.

[1] *European Organization for Nuclear Research* near Geneva, Suisse

2 Theoretical Background

The standard model of particle physics (SM) describes the fundamental particles and interactions between them. It is a theory that successfully predicted the existence of several at that time undiscovered particles. In addition, it has been tested extensively in electroweak precision measurements at LEP.
Although the SM shows so far a remarkably successful performance there are also some open questions which can not be answered within the SM. Thus several theories have been developed to address problems which go beyond the SM. One of such well-motivated extensions is supersymmetry (SUSY) for which however no experimental evidence has been found so far.
After a short introduction to the phenomenology of the standard model including a discussion of specific shortcomings, the basic concepts of supersymmetry are introduced in this chapter. In addition, general concepts of searches for supersymmetry at collider experiments are discussed together with a summary of the current status of the results of such searches which have been performed in the past.

2.1 The Standard Model of Particle Physics

The description of the SM comprises the elementary particles and their interactions [1]. In general, one distinguishes between two types of particles: fermions and bosons. While matter particles are fermions with half-integer spin, the fundamental forces are mediated via bosons carrying integer spin. An overview of the contents of the SM is given in Fig. 2.1 where the particles are denoted together with their interactions [1].
Mathematically the standard model is a quantum field theory where interactions between particles are described via gauge symmetries. The underlying gauge group of the standard model is

$$SU(3)_C \otimes SU(2)_L \otimes U(1)_Y$$

where $SU(3)$ is the gauge group of the strong force and C indicates that this force acts on the colour charge, $SU(2)$ represents the weak force and L denotes that this force only acts on left-handed fermions, while $U(1)$ represents the electromagnetic force acting on the hypercharge Y.
A brief description of the properties of the particles contained in the SM and the corresponding interactions is given in the following:

Matter Constituents: In the SM, one distinguishes between twelve different fermions being the elementary constituents of matter. For each fermion there exists also an antiparticle which carries the opposite signed quantum numbers.

[1] Gravity is not included in the current representation of the standard model and thus it is not discussed in this thesis.

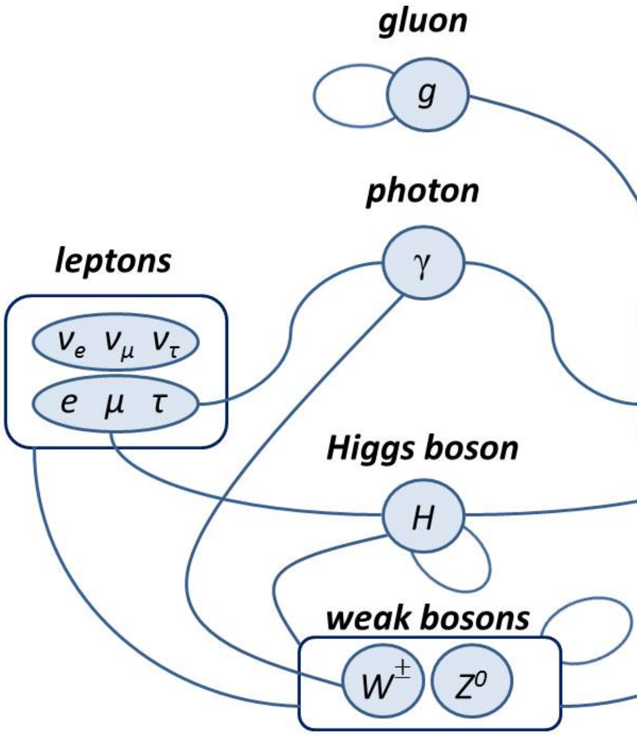

Figure 2.1: Overview of particles contained in the standard model. Blue lines indicate interactions between different particles.

Leptons: The SM contains in total six leptons which are three negatively charged leptons (e, μ, τ) and three neutral leptons (ν_e, ν_μ, ν_τ), the neutrinos. In addition to the charge, leptons are also distinguished according to the lepton numbers which are electron number $L_e = 1$ for electron and electron-neutrino, muon number $L_\mu = 1$ for muon and muon-neutrino and tauon number $L_\tau = 1$ for tauon and tauon-neutrino. Each pair of lepton and neutrino carrying the same lepton number is forming a so-called *generation* where e and ν_e belong to the first generation, μ and ν_μ to the second and τ and ν_τ to the third, respectively.

Quarks: The remaining six fermions in the SM are quarks and can be grouped into generations analogous to the leptons. The first generation is populated by up- and down-quark (u, d), the second by charm- and strange-quark (c, s) and the third by the top- and bottom-quark (t, b). All quarks carry electrical charge but different than for leptons it is not integer but $+2/3$ for the up-type quarks (u, c, t) and $-1/3$ for down-type quarks (d, s, b). Besides to the electrical charge, quarks also carry color charge which comes in three types.

In addition to the attributes described above, fermions are furthermore characterized by the weak isospin. Left-handed fermions in each generation form an isodoublet with a weak isospin of $\pm 1/2$ while right-handed components are isosinglets with a weak isospin of 0.

Fundamental Forces: Matter particles interact with each other through fundamental forces mediated via gauge bosons. These bosons arise from the principle of local gauge invariance under symmetry transformations.

Electromagnetic Force: The description of the electromagnetic force is based on the theory of *Quantum Electrodynamics* (QED). It is communicated between electrically charged particles, like the charged leptons and quarks, by the exchange of photons. These are massless and electrically neutral resulting in the property that the electromagnetic force is long ranged.

Weak Force: The weak force acts on the weak charge which is carried by all fermions in the SM. It is mediated by three vector bosons – namely the two charged $W^{\pm}$ bosons and the neutral Z boson. These bosons are unlike the photon massive with masses of $W^{\pm} = 80.385 \pm 0.015$ GeV and $Z = 91.1876 \pm 0.0021$ GeV [1]. As a result the weak interaction is suppressed with respect to the electromagnetic force.
Weak interactions preferably take place within one generation, e.g. e or μ transform into the respective neutrinos when emitting a W^{-}. However, since the mass eigenstates in the weak interaction differ from the flavour eigenstates, $W^{\pm}$ bosons can also couple to fermions between different generations. In the quark-sector typically a representation is chosen where the up-type flavour eigenstates correspond to the mass eigenstates and the down-type quarks mix. This mixing is described by the CKM-matrix [2,3]. This is an unitary matrix, described by three mixing angles and one CP-violating phase, which indicates the relative strength between individual transitions.

Strong Force: The theoretical framework describing the strong force is called Quantum Chromodynamics (QCD). It is mediated via eight massless gluons and acts on the colour charge which is carried for instance by quarks. In contrast to the photon which is electrically neutral and thus can not interact with itself, gluons carry a colour charge and hence are able to couple to themself. The colour charge exists in three different states commonly denoted as 'red', 'green' and 'blue'. Quarks and gluons are collectively referred to as partons.
Regarding the dependence on the distance the strong force behaves differently than other fundamental forces: the coupling strength increases with rising distance. This is a consequence of the different colour states and the self-coupling property of gluons. It is usually referred to as *confinement* [4] and causes the effect that coloured objects can not exist freely. In fact when separated, coloured objects start to build new coloured particles until only a colour neutral formation is left. Such colourless objects linked by the strong force are named hadrons. On the other hand, particles taking part in the strong interaction start to behave quasi-free when they are brought close together. This feature is known as *asymptotic freedom* [5,6].

First proposed by Salam, Glashow and Weinberg [7, 8], the electromagnetic and the weak force could be successfully unified into the electroweak force. As denoted earlier, the weak force acts on the weak isospin T_3 while the electromagnetic force acts on the hypercharge Y. These two quantities are connected via the following relation to the electric charge Q

$$Q = T_3 + Y/2$$

In the electroweak theory, three gauge bosons $W_\mu^{1,2,3}$ are introduced for $SU(2)_L$ and one gauge boson B_μ for $U(1)_Y$. The physical states photon, $W^\pm$ and Z are formed by mixing of these massless states. While the charged $W_\mu^\pm$ bosons are superpositions of W_μ^1 and W_μ^2, the fields A_μ of the photon and Z_μ of the neutral vector boson are obtained by a mixing of the gauge fields W_μ^3 and B_μ parametrized by the weak mixing angle θ_W . Formel?

Higgs Boson: The electroweak theory in the current representation requires that fermions and bosons are massless particles as mass terms violate the gauge invariance under $SU(2)_L \otimes U(1)_Y$ transformations. This is in contradiction to experimental observations which have shown that all particles, except for photon and gluon, in fact have mass.

An explanation for the generation of particle masses without violation of the principles of the electroweak theory is provided by the *Higgs-mechanism* [9–11] which is based on the concept of spontaneous symmetry breaking. The main idea behind this meachnism is that in general the principle of local gauge invariance is obeyed, but that it is explicitly broken by the ground state. In the context of the Higgs-mechanism this is realized by the introduction of the Higgs field described by a potential with a non-zero minimum value . This non-vanishing minimum represents Formel? the expectation value of the quantum field in the vacuum – the vacuum expectation value. The masses of particles are eventually generated by the couplings to the Higgs field.

Furthermore, the Higgs-mechanism also predicts the existence of a new heavy boson, the Higgs boson, which is a quantum excitation of one of the components of the Higgs field. It is supposed to be a scalar and the Higgs mass one of the free parameters of the SM.

The discovery of a new boson at a mass of around 125 GeV has been announced by the ATLAS and CMS collaborations in 2012 [12, 13]. As all properties of this new boson are consistent with SM predictions so far (c.f. e.g. [14–17]), this indicates that the last remaining gap of the SM could finally be closed.

2.1.1 Limitations of the Standard Model

Although the SM has been incredibly successful so far and lead to several discoveries while withstanding numerous precision tests, it is known to be on the other hand also an incomplete theory. Some of known shortcomings of the SM are discussed in some detail in the following.

Gravity: As stated already earlier, the SM contains no description of gravity. In particular, it is currently not possible to unify general relativity and quantum theory in one common concept.

Matter antimatter asymmetry: According to the SM matter and anitmatter exist to equal amounts in the universe which is in fact not the case. A theory which would be able to explain such an asymmetry needs some source of CP-violation.

The only source of CP-violation within the SM is arising from the CKM matrix as described in 2.1. However, this is not enough to be able to explain the degree of matter antimatter asymmetry in the universe [18].

Unification of couplings: The unification of the electromagnetic and the weak force leads to the question, if it is even possible to further unify the electroweak force with the strong force in order to build a combined theory usually referred to as Grand Unified Theory (GUT). This would imply that the coupling constants of the SM intersect when extrapolating them from the electroweak to the GUT scale. However, this feature is not observed within the SM.

Origin of dark matter and dark energy: There exist several cosmological observations that indicate that the matter described by the SM makes up only 4.9% of the universe [19]. A by far larger part of 26.8% is assigned to so-called *dark matter* which is presumably neutral and only weakly interacting. The only particles within the SM possessing such attributes are neutrinos. However, they are not able to account for the whole relic density present in the universe [20]. Furthermore, for the major part of the universe making up 68.3% there is no hint at all what its' nature could be. Thus it is typically denoted with *dark energy*.

Hierarchy problem: The observable mass of the Higgs boson is given by the bare mass of the Higgs boson plus contributions arising from higher order corrections caused by each massive SM particle. These higher order corrections are usually dependent on an ultraviolet cut-off scale . Conventionally this UV cut-off scale is chosen to be Formel? the Planck scale. This would result in a Higgs mass considerably larger than the oberserved mass of around 125 GeV and requires an enormous amount of fine tuning in order to address this problem.

2.2 Supersymmetry

In order to overcome the weaknesses of the SM and to provide explanations for so far unsolved problems of which some have been dicussed in 2.1.1, several theories have been developed which go beyond the SM. Among those, a favoured extension is *supersymmetry* (SUSY) as it is able to provide several benefits at once. In this section a brief introduction to the general concept of supersymmetry is given with focus on the *Minimal Supersymmetric Standard Model* (MSSM). For detailled reviews see e.g. [21, 22].

The basic idea of a supersymmetric theory is that a fermionic state is converted into a bosonic state and vice versa by the generator of a supersymmetry transformation Q according to

$$Q\,|\text{fermion}\rangle = Q\,|\text{boson}\rangle\,, \qquad\qquad Q\,|\text{boson}\rangle = Q\,|\text{fermion}\rangle\,.$$

The supersymmetric fermionic and bosonic partner particles are called *superpartner* and form together the irreducible representations of the supersymmetry algebra named *supermultiplets* with the same number of fermionic and bosonic degrees of freedom. In case of unbroken supersymmetry, partner particles within one supermultiplet have the same mass as well as the same quantum numbers like electric charge, weak isospin and color degrees of freedom, except for the spin. Commonly, supersymmetric particles are denoted *sparticles*.

Furthermore, in a general supersymmetric theory fulfilling the criteria of gauge invariance and renormalisability, processes are allowed violating either the lepton or baryon number conservation. However, such a process has not been observed experimentally so far and would imply for instance a rapid decay of protons. The current lower limit on the proton lifetime is ... and indicates that such processes must be suppressed. In order to achieve this, a new quantum number called *R-parity* is introduced according to Quelle

$$R = (-1)^{3(B-L)+2S}$$

with baryon number B, lepton number L and spin S. It is a multiplicative quantum number and amounts to $R = +1$ for SM particles while it is $R = -1$ for supersymmetric particles. Assuming R-parity conservation no baryon or lepton number violation processes occur [2]. In addition, the assumption of R-parity conservation leads to further phenomenological implications: Quelle RPV SUSY in Fussnote

- SUSY particles can only be produced in pairs at collider experiments as only even numbers of supersymmetric particles can occur in an interaction vertex.
- The lightest supersymmetric particle (LSP) is stable and thus any decay chain of a supersymmetric particle finally ends in a state containing an odd number of LSPs.

A R-parity conserving supersymmetric theory as described above provides some elegant solutions to open questions as raised in section 2.1.1. As discussed there, the Higgs mass suffers from quadratically divergent contributions arising from higher order corrections caused by SM particles. However, since in SUSY each SM particle gets a supersymmetric partner these higher order corrections cancel as all supersymmetric particles contribute in an unbroken theory with equal size but opposite sign as their corresponding SM partner. Thus SUSY is able to provide a solution to the hierarchy problem. But the observation of such kind of supersymmetric particles with the exact same masses as their SM correpondents would have happened already. Since this is not the case, one knows from all experimental results that supersymmetry in fact has to be a broken symmetry. In order to still be able to provide a solution to the hierarchy problem, supersymmetric particles are expected to be not heavier than $\mathcal{O}(1\,\mathrm{TeV})$. This is the main argument why one would expect supersymmetric particles to be in the TeV range, well within the reach of the LHC. Especially the superpartner of the top quark is expected to be not too heavy in order to be able to cancel the contributions from top loops. This is necessary as these give the largest contributions since the top quark is the heaviest particle in the SM.

In addition to this naturalness aspects, the coupling constants of the forces which do not intersect within the SM actually meet in one point when extrapolating the couplings from the electroweak to the GUT scale considering the existence of supersymmetric particles. This effect is illustrated in Fig. 2.2. It is visible that the evolution of the couplings is modified with respect to the SM at that energy scale where the supersymmetric particles enter. In general, this hints to the possibility of a grand unification.

[2] There exist also several R-parity violating SUSY models which are not in contradiction to the observed proton lifetime. However, these are not subject of this thesis and thus not discussed.

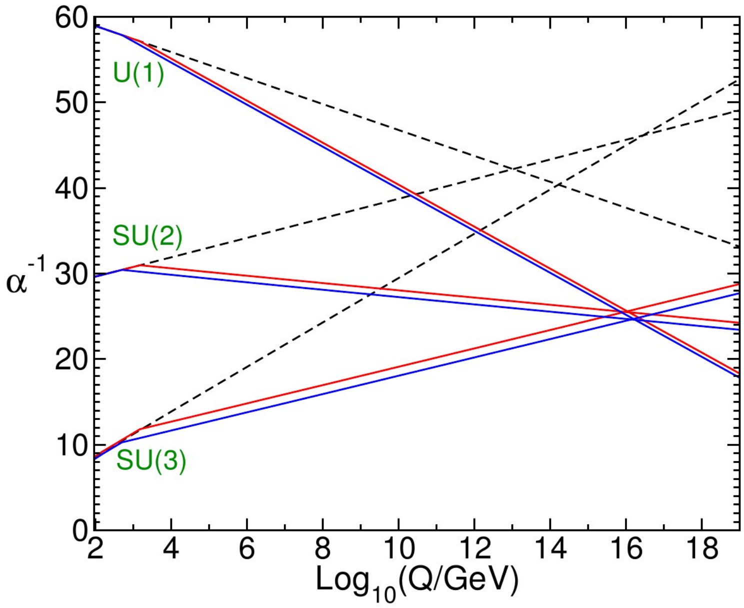

Figure 2.2: Comparison of the renormalization group evolution of the couplings α_a^{-1} in the SM (dashed lines) and the MSSM (solid lines) including two-loop effects. The masses of the supersymmetric particles in the MSSM are considered as a common threshold changing between 500 GeV and 1.5 TeV while $\alpha_3(m_Z)$ is varied between 0.117 and 0.121. Taken from [22].

Besides the two advantages discussed above, R-parity conserving SUSY models also provide a suitable dark matter candidate. As discussed previously, each decay of supersymmetric particles finally leads to the existence of an LSP which can not decay further. Thus, it is an adequate DM candidate when it is electrically uncharged and only weakly interacting.

2.2.1 The MSSM

The smallest possible supersymmetric extension of the SM including the full particle spectrum and interactions is comprised in the MSSM. An overview of the respective particle content is given in Tab. 2.2.1. This extension is minimal in that sense that it introduces the least feasible number of additional particles to the existing SM particles. Thus, each SM fermion gets an individual superpartner while the interactions and couplings of the supersymmetric particles are the same as for the SM counterparts. The different transformation of left- and right-handed fermions under the gauge groups implies the necessity to introduce separate superpartners for left- and right-handed states as well. These are arranged with their bosonic (spin 0) superpartner in a *chiral* supermultiplet. The labels indicating the left- and right-handed states refer to the helicity of the respective SM particle. These supersymmetric partners of fermions are named *sfermions* distinguishing between *sleptons* and *squarks* – the supersymmetric partners of leptons and quarks. In a similar manner the SM gauge bosons are arranged in *gauge* supermultiplets together with their fermionic (spin 1/2) supersymmetric correspondents. The SUSY partners of the gauge

Type	Spin	Gauge eigenstates	Mass eigenstates
Higgs bosons	0	$H_u^0\ H_d^0\ H_u^+\ H_d^-$	$h^0\ H^0\ A^0\ H^\pm$
Squarks	0	$\tilde{u}_L\ \tilde{u}_R\ \tilde{d}_L\ \tilde{d}_R$ $\tilde{s}_L\ \tilde{s}_R\ \tilde{c}_L\ \tilde{c}_R$ $\tilde{t}_L\ \tilde{t}_R\ \tilde{b}_L\ \tilde{b}_R$	see left see left $\tilde{t}_1\ \tilde{t}_2\ \tilde{b}_1\ \tilde{b}_2$
Sleptons	0	$\tilde{e}_L\ \tilde{e}_R\ \tilde{\nu}_e$ $\tilde{\mu}_L\ \tilde{\mu}_R\ \tilde{\nu}_\mu$ $\tilde{\tau}_L\ \tilde{\tau}_R\ \tilde{\nu}_\tau$	see left see left $\tilde{\tau}_1\ \tilde{\tau}_2\ \tilde{\nu}_\tau$
Neutralinos	1/2	$\tilde{B}^0\ \tilde{W}^0\ \tilde{H}_u^0\ \tilde{H}_d^0$	$\tilde{\chi}_1^0\ \tilde{\chi}_2^0\ \tilde{\chi}_3^0\ \tilde{\chi}_4^0$
Charginos	1/2	$\tilde{W}^\pm\ \tilde{H}_u^+\ \tilde{H}_d^-$	$\tilde{\chi}_1^\pm\ \tilde{\chi}_2^\pm$
Gluino	1/2	$\tilde{g}$	see left
Gravitino	3/2	$\tilde{G}$	see left

Table 2.1: Supersymmetric particles contained in the MSSM neglecting mixing in the first two sfermion generations. Following [22].

bosons are named *gauginos* so that the superpartners in the gauge supermultiplets are the *gluino*, *wino* and *bino*. The corresponding gaugino mixtures of the neutral wino and the bino are the *photino* and the *zino*. Beyond that, the supersymmetric particle spectrum is extended by another supermultiplet containing the graviton (spin 2) and the respective supersymmetric partner – the *gravitino* (spin 3/2).

As described in Sec. 2.1, masses arise in the SM from the concept of spontaneous symmetry breaking implying the existence of the Higgs boson. The supersymmetric partner of the Higgs boson is named *higgsino*. While in the SM one Higgs doublet is sufficient to give mass to all particles, the Higgs sector needs to be extended in the MSSM. Here, two Higgs doublets are introduced where one doublet H_u gives mass to the up-type quarks and the other one H_d to the down-type quarks, respectively. These two doublets have together eight degrees of freedom of which three are needed to give mass to the gauge bosons of the weak interaction as in the SM. This results in five physical Higgs bosons which are the two scalar Higgs particles h^0, H^0, the pseudoscalar A^0 as well as the charged Higgs bosons $H^\pm$. As further consequence there are two vacuum expectation values v_u and v_d present – each assigned to one Higgs doublet whose ratio $\tan\beta = v_u/v_d$ is a free parameter of the model.

As in the SM, the gauge eigenstates of the theory do not necessarily have to be also the mass eigenstates. A mixing occurs especially in the gaugino sector. Here, the neutral components of the bino and wino mix with the neutral higgsinos and form four mass eigenstates – the *neutralinos* $\tilde{\chi}^0$. Similarly, also the charged gauginos and higgsinos mix to the four *charginos* $\tilde{\chi}^\pm$. Furthermore, mixing can also appear in the third squark and slepton generation.

All in all, the MSSM introduces 35 new particles (neglecting mixing in the two first fermion generations) and possesses 124 free parameters of which 18 correspond to SM parameters [1].

2.2.2 SUSY-Breaking

2.2.3 Searches for Supersymmetry at Collider Experiments

SUSY is easy to search for at colliders. That is why we do it...bla bla bla bla bla

- how do we search at colliders?
- searches at previous experiments
- status: 7 TeV cmssm
- cross sections at 8 tev

3 Experimental Setup

In order to probe the various aspects of the well-established standard model or search for hints of new physics beyond the SM, particle physics experiments preferentially make use of powerful particle accelerators where particles of a certain type are collided in order to probe the constituents of matter and interactions between them. The analyses presented in this thesis are all performed in the context of the CMS experiment located at the Large Hadron Collider (LHC) at CERN near Geneva.
The first part of this chapter provides an introduction to the LHC. This is followed by an overview of the detector system of the CMS experiment. Afterwards the hitherto periods of collision data taking at the LHC are discussed together with an introduction to the generation of simulated events which are used in the analysis of real data events.

3.1 The Large Hadron Collider

The Large Hadron Collider [23, 24] is a ring-accelerator designed to provide particle collisions of hadrons. It is built in the tunnel of the former LEP [25] collider 45 – 170 m below the ground and has a circumference of 26.7 km. The LHC is a particle-particle collider and thus composed of two rings with counter-rotating beams. The operation can be performed in different modes with either proton beams or heavy ions like e.g. lead [1].
In each beam, protons are grouped together in bunches and accelerated in two evacuated beam pipes using superconducting radio-frequency cavities. With a nominal bunch spacing of 25 ns the bunch revolution frequency is 40 MHz. Each of the 2808 individual bunches per beam contains at design conditions 1.15×10^{11} protons. In order to bend the beams around the LHC ring superconducting dipole magnets are used with an operation temperature of 1.9 K. They provide a magnetic field of up to 8.33 T while additional quadrupole and sextupole magnets are utilized to squeeze and focus the beams.
Before the protons are injected into the LHC they are already pre-accelerated in various smaller accelerators up to a beam energy of 450 GeV while passing through the injector chain Linac2 – Proton Synchrotron Booster (PSB) – Proton Synchrotron (PS) – Super Proton Synchrotron (SPS). An overview of the accelerator complex at CERN is given in Fig. 3.1.

The main goal of the LHC is to provide proton-proton collisions to the experiments with center of mass energies up to 14 TeV in order to explore physics processes at novel energy regimes. The expected number of events N for a certain type of process is given by the product of the specific cross section σ of that process and the integral $L = \int \mathcal{L}\, dt$ of the instantaneous luminosity $\mathcal{L}$ over time such that

$$N = \sigma \cdot L. \tag{3.1}$$

[1] All studies presented in this thesis are based on proton-proton collisions. Thus the operation with heavy ions is not discussed.

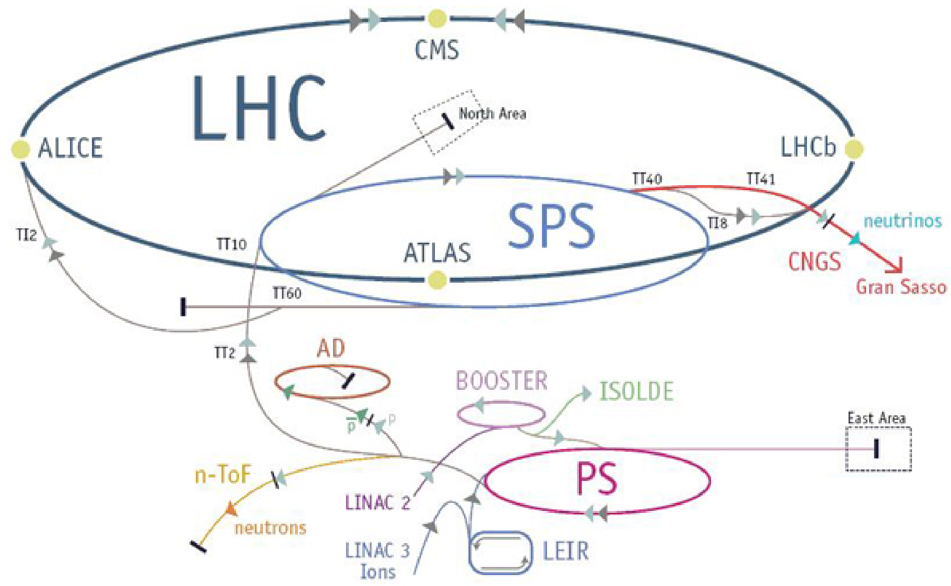

Figure 3.1: Illustration of the CERN accelerator complex including the injector chain of the LHC ring. Taken from [26].

The luminosity is a machine parameter and can be expressed for beams with Gaussian-shaped profiles as

$$\mathcal{L} = \frac{f n_1 n_2}{4\pi\sigma_x\sigma y} \cdot F \tag{3.2}$$

with the revolution frequency f, the number of particles n_1 and n_2 contained in the two colliding bunches and the transverse beam sizes σ_x (σ_y) in the horizontal (vertical) directions. In order to take the inclination of the two beams into account, the geomatrical correction factor F is introduced. The nominal peak luminosity of the LHC is $10^{34}\,\mathrm{cm}^{-2}\,\mathrm{s}^{-1}$. Since the total inelastic proton-proton cross-section at a center of mass energy of 14 TeV is close to 100 mb as indicated in Fig. 3.2, the expected event rate is approximately 10^9 events per second. This is resulting in high technical challenges for the experiments.

The four main experiments are located at the four locations along the LHC ring where the beams cross in order to measure the delivered particle collisions. The two high luminosity experiments ATLAS [28] and CMS [29, 30] are designed for multiple purposes like precision measurements of SM quantities, search for the standard model Higgs Boson or searches for signals indicating new physics processes. The LHCb detector [31] however is a specialised experiment focusing on the measurement of CP violation in the interactions of hadrons containing b-quarks. The only experiment designed especially for the analysis of heavy ion collisions is the ALICE [32] detector with the main emphasis on the physics of strongly interacting matter at extreme energy densities like for instance quark-gluon plasma.

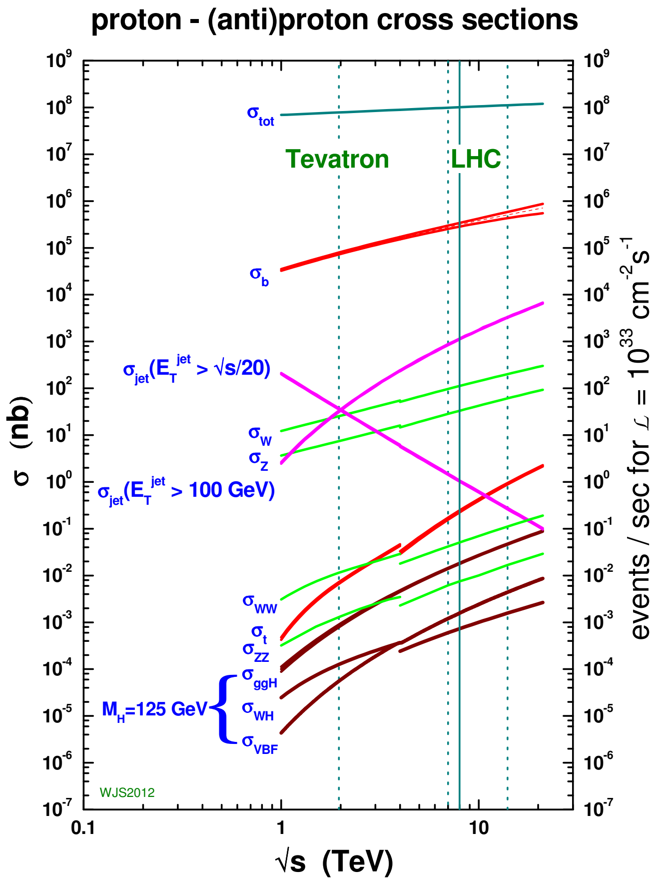

Figure 3.2: Summary of cross sections for various standard model processes in proton-proton and proton-antiproton collisions as function of the centre of mass energy. The right axis displays the correponding event rate at a luminosity of $10^{33}\,\mathrm{cm}^{-2}\mathrm{s}^{-1}$. Taken from [27].

3.2 The CMS Experiment

The CMS detector is one of the two experiments at the LHC designed to address a multitude of physics questions. In addition to tests of the SM at the TeV scale, studies of the nature of elektroweak symmetry breaking which might show up in the presence of a Higgs boson and searches for so far unknown particles pointing to e.g. new symmetries in nature are the primary targets of these experiments. These ambitious physics goals can only be achieved by fully exploiting the by now unprecedented collision energy and luminosity.

The CMS detector with its typical cylindrical design of different sub-detector components around the beam line is designed to perfectly meet these particular conditions. A sketch of the CMS detector and the different sub-detectors is shown in Fig. 3.3. As a typical high-energy particle experiment the CMS detector makes mainly use of tracking

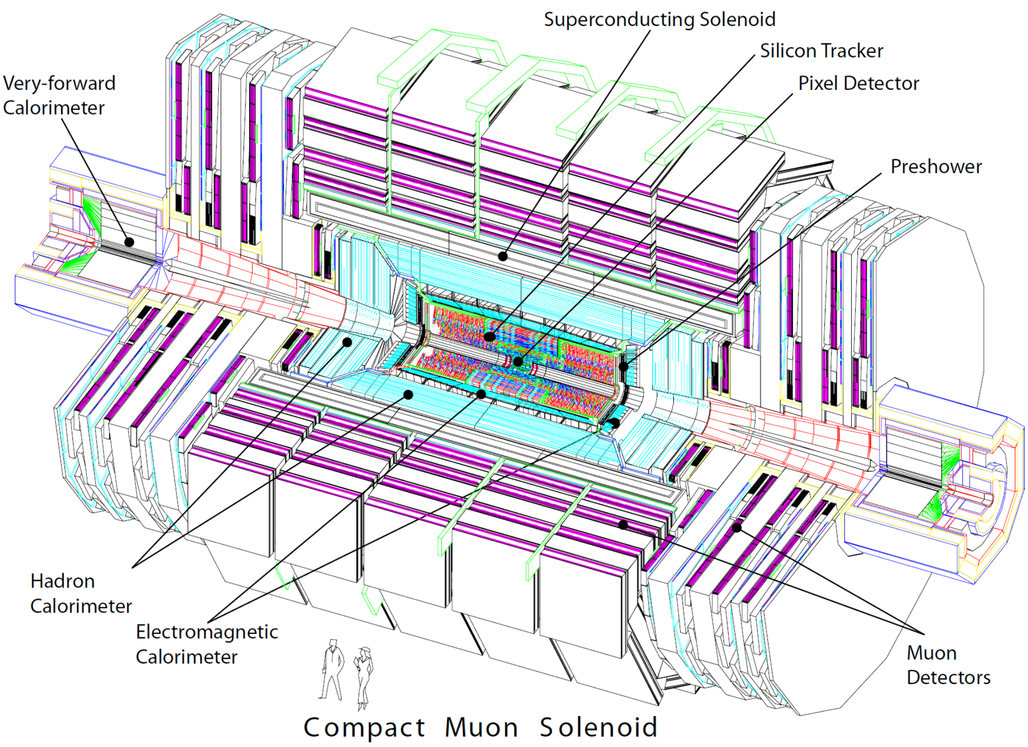

Figure 3.3: A perspective view of the CMS detector [29].

detectors and calorimeters to measure particles' momenta, energy depositions and flight directions in order to identify the objects emerging from the particle collisions. The entire CMS detector with a length of 21.6 m and a diameter of 14.6 m results in a total weight of 12500 t.
The following sections comprise a description of the CMS detector and individual sub-detector components focusing on the detector parts most relevant for the analyses presented in this thesis. A detailed discussion of the detector design can be found in [29, 30].

3.2.1 Coordinate Conventions and Kinematic Variables

In order to describe the particle collisions, the CMS experiment makes use of a right-handed coordinate system with its origin at the center of the detector at the nominal interaction point. While the z-axis is defined along the direction of the beam, the x-axis points to the center of the LHC ring and the y-axis vertically upwards. In this xy-plane the azimuthal angle ϕ is measured where $\phi = 0$ coincides with the x-axis. The polar angle θ however is defined with respect to the z-axis. A quantity closely related to the polar angle is the pseudorapidity η defined as

$$\eta = -\ln\left[\tan\left(\frac{\theta}{2}\right)\right] \tag{3.3}$$

which is widely used in experimental particle physics as rapidity differences are Lorentz invariant. A pseudorapidity $\eta = 0$ corresponds to the direction perpendicular to the beam while $|\eta| \rightarrow \infty$ points along the beam. Based on the pseudorapidity the Lorentz invariant distance between two objects $\Delta\mathrm{R}$ can be written as

$$\Delta\mathrm{R} = \sqrt{(\Delta\eta)^2 + (\Delta\phi)^2}\,. \tag{3.4}$$

At the LHC the initial conditions of the primary collisions are not known as the specific energy fraction of the proton which each parton carries can not be identified. Thus conservation of the total momentum can not be utilized directly to describe the momentum balance in the final state. However, it is known that the initial particles have no significant momentum orthogonal to the beam axis which is referred to as transverse momentum

$$p_\mathrm{T} = p \cdot \sin\theta\,. \tag{3.5}$$

Thus, momentum conservation in the transverse plane is used to describe the final state conditions. Any difference between the total sum of all transverse momenta and zero is considered as missing energy $\not{E}_\mathrm{T}$ and often exploited to describe undetected particles.

3.2.2 Superconducting Magnet

The CMS experiment makes use of a large superconducting solenoid magnet which is a crucial component of the whole detector design and provides a magnetic field of up to 4 T. It allows to precisely determine the momenta and charge of charged particles from the bended tracks that they follow in the magnetic field.
With a length of 12.5 m and a diameter of the free bore of 6.3 m the total cold mass reaches 220 t. It is made up of a niobium-titanium coil which is winded in 4-layers. This configuration allows a storage of 2.6 GJ energy at full current. A 10000 t heavy-weight iron yoke is responsible for the return of the magnetic flux.

3.2.3 Inner Tracking System

The tracking system of the CMS experiment is the innermost part of the detector and installed directly around the interaction point completely contained in the bore of the magnet system. Its' purpose is to precisely measure the trajectories of charged particles arising from the collisions as well as to reconstruct secondary vertices. Due to the location close to the interaction point the tracking system has to cope with a high particle flux crossing the tracker associated with each bunch crossing. Hence high requirements on response time and granularity are set in order to properly identify the particles' tracks.
In order to fulfill these tasks the CMS experiment makes use of a tracker design based on silicon detectors. It consists of mainly two components: the innermost part is made of silicon pixel detectors while these are surrounded by silicon strip modules. In total they add up to an active area of 200 m^2 with a length of 5.8 m and a diameter of 2.5 m covering the detector up to $|\eta| = 2.5$. A schematic overview of the whole tracking system is shown in Fig. 3.4.

Pixel Detector: The pixel detector consists of three barrel layers which extend from 4.4 cm to 10.2 cm and two endcap disks on each side. In total there are 1440 pixel modules installed. The size of one pixel cell is 100 x 150 μm^2 providing similar track

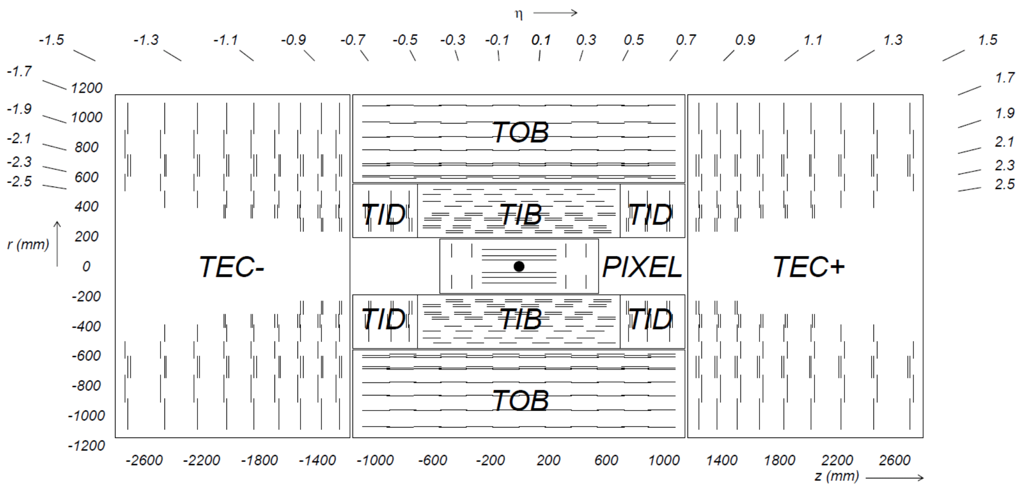

Figure 3.4: Sketch of the CMS tracking system in a rz-view. Each tracker module is represented by one line. Taken from [29].

resolution quality in $r-\phi$ and z direction. This configuration provides for almost the whole range up to $|\eta| = 2.5$ three precise tracking hits. This is especially important for the reconstruction of secondary vertices.

Silicon Strip Tracker: The silicon strip detector which extends to a radius of 1.1 m comprises the pixel tracker. The more than 15000 individual strip detector modules are arranged in an inner and an outer detector part. The inner part of the strip tracker is build by the four Tracker Inner Barrel (TIB) layers which are accompanied by the three Tracker Inner Disks (TID) at the end sides. This inner part provides up to four track measurements in the $r-\phi$ plane. The TIB/TID system lies within the Tracker Outer Barrel (TOB) consisting of another six barrel layers while it is complemented by the Tracker EndCaps (TEC) which add another nine disks at each side of the tracking system. This layout provides at least around nine hits within the silicon strip system.

The tracking system with the desgin described above provides a very good impact parameter resolution and tracking efficiency [33]. The impact parameter resolution is of the order of $< 35\,\mu$m in the plane perpendicular to the beam (for particles with $p_{\mathrm{T}} > 10\,$GeV) and reaches $75\,\mu$m in the longitudinal direction. Also the track reconstruction efficiency is expected to show a very good performance. The track reconstruction efficiency of high energetic electrons is above 90%, that of charged hadrons up to 95% (for $p_{\mathrm{T}} > 10\,$GeV) and that for muons even better than 98% in the whole covered region up to $|\eta| = 2.5$ already for muons with very low transverse momenta around 1 GeV. Altogether, the relative transverse momentum resolution reaches a level of 1-2% for high momentum tracks ($\approx 100\,$GeV) in the central barrel for $|\eta| < 1.6$.

3.2.4 Electromagnetic Calorimeter

The CMS experiment makes use of a homogeneous electromagnetic calorimeter (ECAL) in order to precisely measure the energy deposits of electrons and photons. It is installed

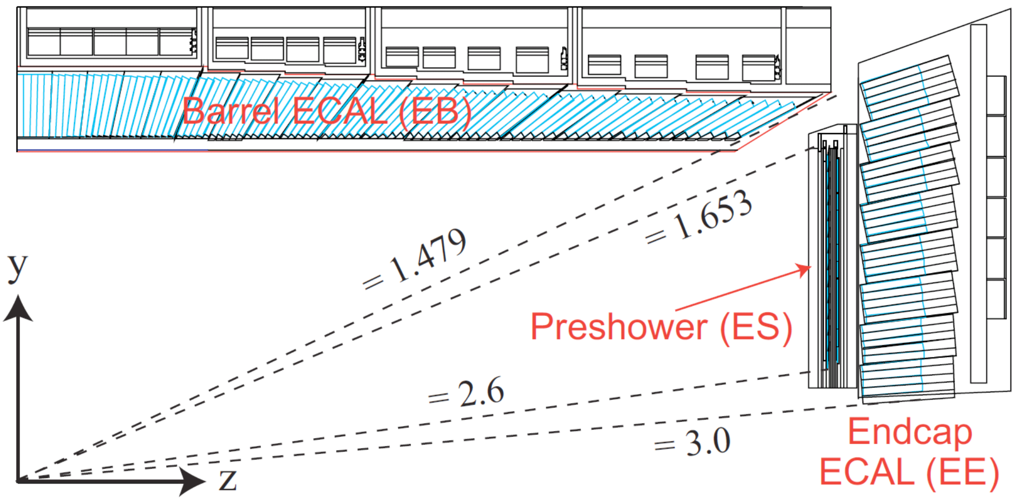

Figure 3.5: View of one quarter section of the CMS electromagnetic calorimeter in a yz-view. Taken from [30].

around the inner tracking system covering a range up to $|\eta| = 3.0$ and consists of lead tungstate ($PbWO_4$) crystals. These have been chosen as they provide a high density, short radiation length and a small Molière radius and hence allow to build a compact calorimeter with a fine granularity. As 80% of the scintillation light is emitted within 25 ns, this matches well the bunch crossing rate of the LHC machine. In order to collect the radiated light photodiodes are glued to the back of each crystal.
An overview of the ECAL layout is shown in Fig. 3.5. The individual sub-components are the following:

Barrel ECAL (EB): The barrel detector of the ECAL covers the pseudorapidity region up to $|\eta| = 1.479$. Within a radius of about 1.3 m a total number of 61200 crystals are installed. Each of them has a length of 230 mm resulting in a radiation length of 25.8 X_0. The crystal cross-section in (η, ϕ) is $(0.0174, 0.0174)$. Avalanche photodiodes are used to detect the emitted scintillation light.

Endcap ECAL (EE): The EB is complemented on each side by an endcap which consists of two d-shaped halfs. The ECAL endcaps extend from $|\eta| = 1.479$ to $|\eta| = 3.0$. In total they contain another 14648 crystals with an individual length of 220 mm corresponding to 24.7 X_0. For the collection of scintillation light vacuum phototriodes are used in the endcaps.

Preshower (ES): In front of the endcap crystals a preshower detector is placed. It covers the pseudorapidity range of $|\eta| = 1.653 - 2.6$. The main purpose is to identify photons emerging from the decay of neutral pions. It is a two-layer sampling calorimeter with lead as absorber material and silicon strip sensors measuring the deposited energy. The total thickness of the preshower is 20 cm (3 X_0).

In order to achieve a stable and uniform energy measurement across the whole ECAL an accurate calibration is of crucial importance. In addition to the calibration of the absolute energy scale especially channel-to-channel effects – referred to as intercalibration –

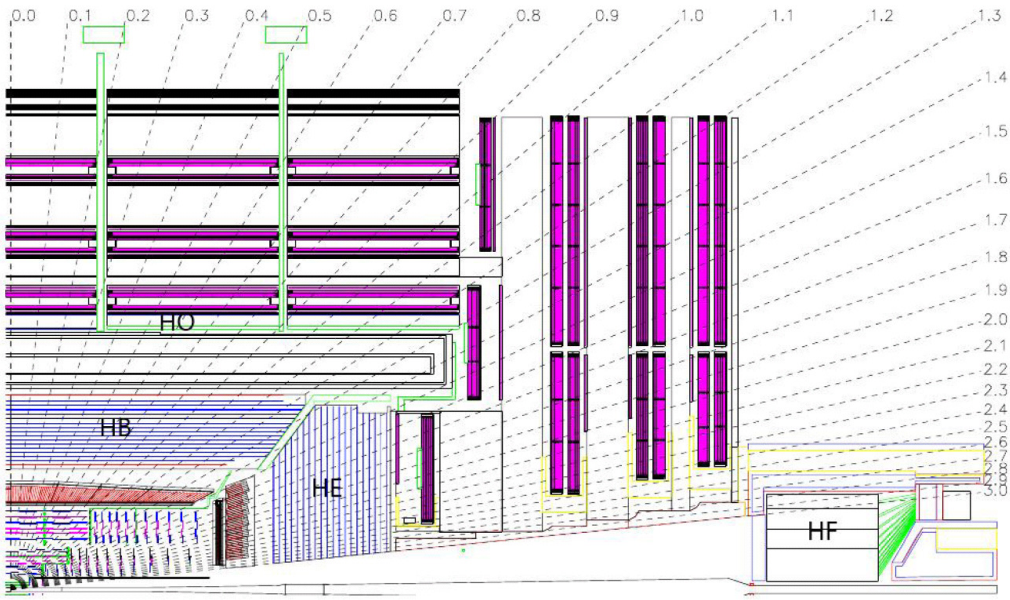

Figure 3.6: Longitudinal view of one quarter of the CMS detector showing the location of the individual HCAL sub-detector parts. Taken from [29].

have to be accounted for which is mainly done based on physics events. Changes in the transparency of the ECAL crystals during operation caused by irradiation are monitored by a dedicated laser system based on the injection of reference laser pulses into the crystals. The typical achievable relative energy resolution for 120 GeV electrons with this calorimeter configuration is of the order of 0.5%.

3.2.5 Hadron Calorimeter

In addition to the previously described electromagnetic calorimeter, the calorimetry of the CMS experiment is completed by the hadron calorimeter (HCAL). It is designed to provide an accurate energy measurement of hadron jets and indirectly also of invisible particles like e.g. neutrinos by the determination of missing transverse energy. In order to obtain a measure of the missing transverse energy it is important that the calorimeter is hermetic in the sense that it provides a large geometric coverage to potentially measure all particles emerging from an interaction. Thus the HCAL is build such that a pseudorapidity range up to $|\eta| = 5.2$ is comprised.

The hadron calorimeter completely surrounds the inner tracking system and the electromagnetic barrel calorimeter while it is mainly contained within the magnet system. Hence its radial dimensions are limited on the one hand by the outer circumference of the barrel ECAL and on the other hand by the inner border of the magnet coil. To ensure that the complete hadronic showers are contained in the HCAL, an additional calorimeter component is installed outside the solenoid in the barrel part.

An overview of the layout of the CMS hadron calorimeter is shown in Fig. 3.6. It is a typical sampling calorimeter with alternating layers of absorber material and active scintillator layers. The individual sub-components are the following:

Hadron barrel (HB): The barrel part of the CMS hadron calorimeter covers the pseudorapidity range up to $|\eta| = 1.3$ and is composed of two half barrels each containing 36 identical azimuthal wegdes. These wedges hold the absorber plates which are flat brass plates arranged parallel to the axis of the beam. For reasons of stability the first and last layers are made of stainless steel. The total thickness of the absorber material ranges from 5.82 interactions lengths (λ_I) at $|\eta| = 0.0$ to 10.6 λ_I at $|\eta| = 1.3$. The 17 active plastic scintillator layers alternate with the absorber plates and have a segmentation in $(\Delta\eta, \Delta\phi)$ of (0.087, 0.087).
Each half barrel is divided into 16 η-regions for which the individual tiles are optically linked together using wavelength shiftig fibres and thus form so-called *HCAL towers*. The read-out of each longitudinal tower is carried out using pixelated hybrid photodiodes.

Hadron outer (HO): The calorimeters in the central pseudorapidity region do not provide a sufficient depth in order to fully contain all hadronic showers. Therefore the HB is complemented by the outer hadron barrel part which is placed outside the solenoid covering $|\eta| \leq 1.26$. The HO makes use of the solenoid as additional absorber material and adds another one or even two layers in the most central part of scintillators to the barrel region. Thus the total depth is extended to 11.8 λ_I.

Hadron endcap (HE): The hadron barrel calorimeter is supplemented by the hadron endcap. It is mounted on the endcap iron yoke and covers the pseudorapidity region of $1.3 \leq |\eta| \leq 3.0$ using 18 scintillator layers inserted into brass absorber plates. The granularity of the endcap calorimeter is the same as for the barrel up to $|\eta| = 1.6$ and gets coarser for larger pseudorapidities with $(\Delta\eta, \Delta\phi) \approx (0.17, 0.17)$.

Hadron forward (HF): The forward hadron calorimeter extends the pseudorapidity coverage from $|\eta| = 2.9$ (slightly overlapping with the HE) up to $|\eta| = 5.2$. It is located 11.2 m from the nominal interaction point and has to be in particular radiation hard to cope with the vast particle flux. Thus the HF is made of steel absorber plates with radiation hard quartz fibres integrated as active material. These fibres are arranged parallel to the beam line and form towers with a size in $(\Delta\eta, \Delta\phi)$ of $\approx$ (0.175, 0.175). The signal is detected as Cerenkov light originating from the quartz fibres.

Similar to the ECAL also the performance of the HCAL has to be well calibrated and further monitored during operation. Thus an initial calibration using a radioactive source is combined with test beam data to derive the absolute energy scale. A continous update of this calibrations is performed using isolated energetic particles e.g. from decays of W or Z bosons.

3.2.6 Muon System

The outermost part of the CMS detector – as seen from the interaction point – is made up of the muon system. This important component of the detector is assembled in the return yoke of the CMS magnet and consists of a central barrel cylinder which is complemented by endcap disks in the forward region. This results in a coverage of the pseudorapidity range up to $|\eta| = 2.4$. In the barrel part four layers of detectors are installed alternating

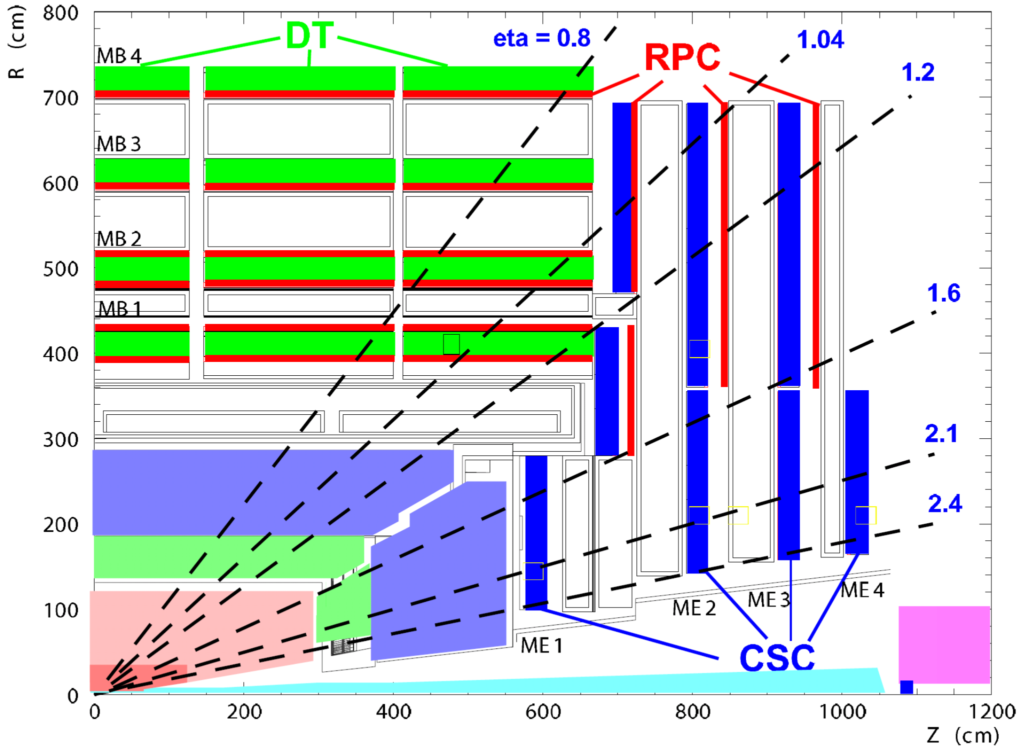

Figure 3.7: Taken from [30].

with the iron yoke while the detectors in the endcap are mounted on four discs perpendicular to the beam. In total about 25000 m^2 detection planes are employed. The layout of the muon system is illustrated in Fig. 3.7.
In order to feature a good muon momentum resolution given the different radiation conditions and variations in the homogenity of the magnetic field depending on the pseudorapidity region it is made use of three different types of gaseous detectors. These different types of tracking chambers are described in the following:

Drift tube (DT) chambers: In the barrel region for $|\eta| < 1.2$ where the background due to neutrons is low and residual effects from the magnetic field likewise the muon system is equipped with drift tube chambers. While in all four stations in the barrel the muon coordinates in the $r\phi$-plane are measured, only the first three layers provide also a measurement of the z-direction. The maximum drift length was chosen to be 21 mm resulting in a negligible occupancy while keeping the number of active channels at an acceptable level. Furthermore, a technology based on tubes was chosen avoiding the issue of possibly broken wires. The resolution in $r\phi$ is designed to reach a precision of 100 μm.

Cathode strip chambers (CSC): The endcap regions are equipped with cathode strip chambers and cover the pseudorapidity range $0.9 < |\eta| < 2.4$. These are chosen as they provide a fast response time and fine segmentation while they are resistant against radiation. Thus they are well suited for the forward region where the muon and background rates are largely increased and the magnetic field is high and nonuniform. The CSCs which are multiwire proportional chambers where anode wires are interlaced with cathode panels perform a precise position measurement in the $r\phi$ bending plane with a spatial resolution of 75-150 μm.

Resistive plate chambers (RPC): Resistive plate chambers are used to complement the drift tube and cathode strip chambers in the range $|\eta| < 1.6$. These are gaseous parallel-plate detectors with a spacial resolution coarser than the DTs and CSCs but usable at high particle rates while providing a very fast response and good time resolution. Thus they are able to very efficiently detect the correct bunch-crossing a muon track is associated to.

The global muon reconstruction efficiency is in general about $95-99\%$ and only drops for some $|\eta|$ regions like e.g. in the transition region between the barrel and endcap part around $|\eta| = 1.2$. Since muons reaching the muon system are affected by multiple scattering the resolution for muons with low transverse momenta below ≈ 200 GeV is in general better based on the inner tracking system than for the muon system alone. For highly energetic muons it is comparable. In general, the muon momentum resolution can be improved by combining the information from the inner tracker and the muon system due to an improved fault finding. This combined approach results in a relative muon momentum resolution for muons with high momenta around 1 TeV of about 5%.

3.2.7 Trigger System

The LHC operating at design conditions provides particle collisions with an interaction rate of 40 MHz. This results in an enormous amount of data events which have to be processed and stored for later offline analyses. With an approximate event size of 1 MB it is technically impossible to record all such events. However, as illustrated in Fig. 3.2 the event rate of interesting potentially new physics events is orders of magnitudes smaller than the proton-proton cross section. Thus, this allows to already perform online a suitable event preselection in order to reduce the amount of data to a storable size still containing the information of interest. Hence, the trigger system also makes up the first step in the physics analysis process.
In order to achieve the necessary rate reduction, the CMS experiment makes use of a two-stage trigger system. This is described in the following.

Level-1 (L1) Trigger: The L1 Trigger consists of custom-made fast programmable hardware. It makes use of data received from fast detector components – namely the calorimeters and the muon system – at reduced granularity. For instance at L1 the calorimeter is divided into so-called *trigger towers* which cover an area in (η, ϕ) of $(0.087, 0.087)$ up to $|\eta| = 1.74$ and get even coarser for higher $|\eta|$. At L1 the trigger decision is based on energy deposits in those trigger towers or certain hit patterns in the muon chambers forming trigger primitive objects as electrons/photons, muons or jets and global quantities like sums of E_{T} or $\not{E}_{\mathrm{T}}$. Events are accepted, if these trigger objects pass some predefined criteria like certain p_{T} thresholds. The L1 trigger latency between the actual bunch crossing and the delivery of the L1 trigger decision to the front-end electronics is $3.2\,\mu s$. During this period the high resolution data is pipelined in readout buffers for further processing. Following this procedure the L1 trigger reduces the event rate to 100 kHz.

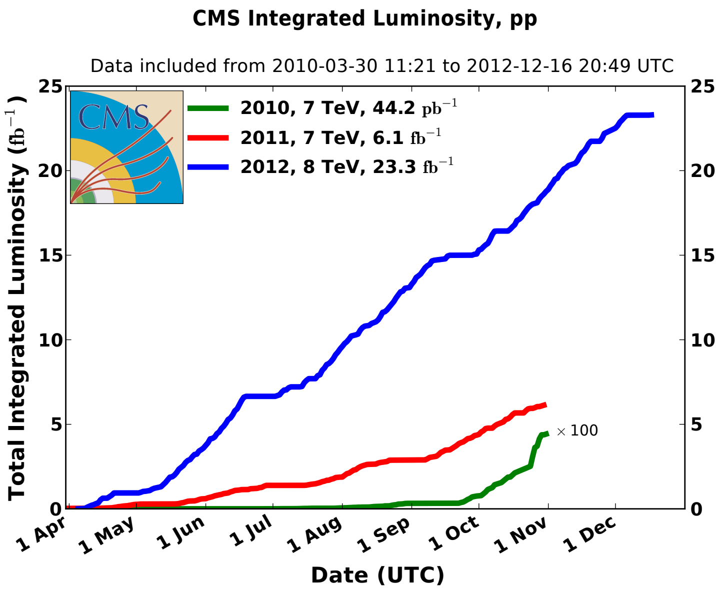

Figure 3.8: Cumulative integrated luminosity versus day delivered to CMS during stable beams for pp collisions. Different data-taking periods are indicated as follows: green for 2010, red for 2011 and blue for 2012. Taken from [34].

High-Level Trigger (HLT): Events that are accepted by the L1 are transferred to the High-Level trigger for further processing. The HLT is a software system running on several thousand commercial processors. It has access to the full information from all sub-detectors and performs an event reconstruction similar to the later offline reconstruction. Thus it allows a further rate reduction to the final output rate of a few hundred Hz of events that are finally stored for analyses. Since the HLT is software based, it allows to continously adjust the used algorithms in order to perfectly meet changing conditions during operation.

3.3 LHC Operation and Data Taking

The LHC was put into operation the first time in September 2008. After a major cooling incident only a few days later requiring a longer technical stop, beams were circulated again in November 2009. The first collisions at a center of mass energy of 7 TeV finally took place end of March 2010 [35]. In the following running period in 2010, data corresponding to an integrated luminosity of 44.2 pb^{-1} were delivered to the experiments with a maximum peak instantaneous luminosity of $2.05 \times 10^{32}\,\mathrm{cm}^{-2}\,\mathrm{s}^{-1}$. These data allowed intense studies of the detector performance and made first searches for new physics possible. The next data taking period performed during 2011 at the same center of mass energy even lead to much more pp collision data provided to the experiments with a total amount of 6.1 fb^{-1} reaching a peak instantaneous luminosity of $3.5 \times 10^{33}\,\mathrm{cm}^{-2}\,\mathrm{s}^{-1}$. Following another technical shutdown during winter, the center of mass energy was finally increased to 8 TeV for the running period during 2012 and the peak luminosity reached with values of up to $7.7 \times 10^{33}\,\mathrm{cm}^{-2}\,\mathrm{s}^{-1}$ already almost design conditions. In total, 23.3 fb^{-1} of integrated

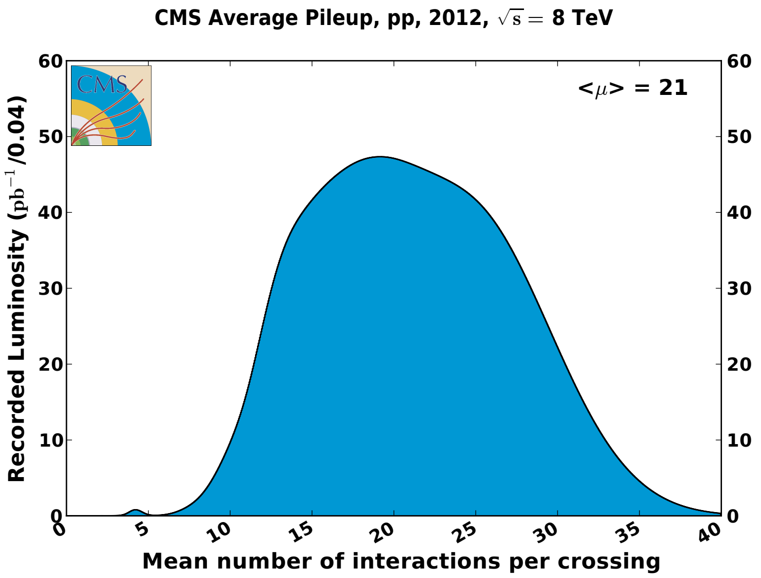

Figure 3.9: Mean number of interactions per bunch crossing in pp collisions at $\sqrt{s} = 8$ TeV. Taken from [34].

luminosity pp collisions were produced by the LHC operating at stable beam conditions. The evolution of the integrated luminosity versus days is also illustrated in Fig. 3.8.

During most of the operation in 2012, the LHC was circulating 1380 bunches per beam with a distance of 50 ns. The average bunch intensity, i. e. the number of protons per bunch, was varying from 1.6 to 1.7×10^{11} extending already the design value [34, 36]. This was on average resulting in 21 pp collisions per bunch crossing. This process of multiple interactions per bunch crossing is known as *pileup*. An overview of the pileup profile observed in collision data taken in 2012 is given in Fig. 3.9. The maximum number of pileup events even reached a value of ≈ 40. This effect caused by the required high luminosity generates challenging conditions for the experiments as many objects arising from such multiple interactions have to be asigned to the correct process and particular collision objects have to be filtered. Dedicated techniques in order to cope with this problem have been developed of which some are discussed in Chapter 4.

3.4 Event Simulation

An important tool in high energy physics is the use of simulation in order to acquire a good understanding of the behaviour of particle collisions and related collision products observed in the detector. Thus, simulated events often serve as benchmark for the development of new detector concepts. Moreover, they are heavily exploited in the validation and interpretation of the results of actual collision experiments, likewise for the LHC. For instance simulated events are used to derive expectations for certain physics properties or the detector performance. In particular they allow to estimate how signals of new physics events would look like in the experiment.

This section provides a brief introduction to the principles of event simulation in hadron

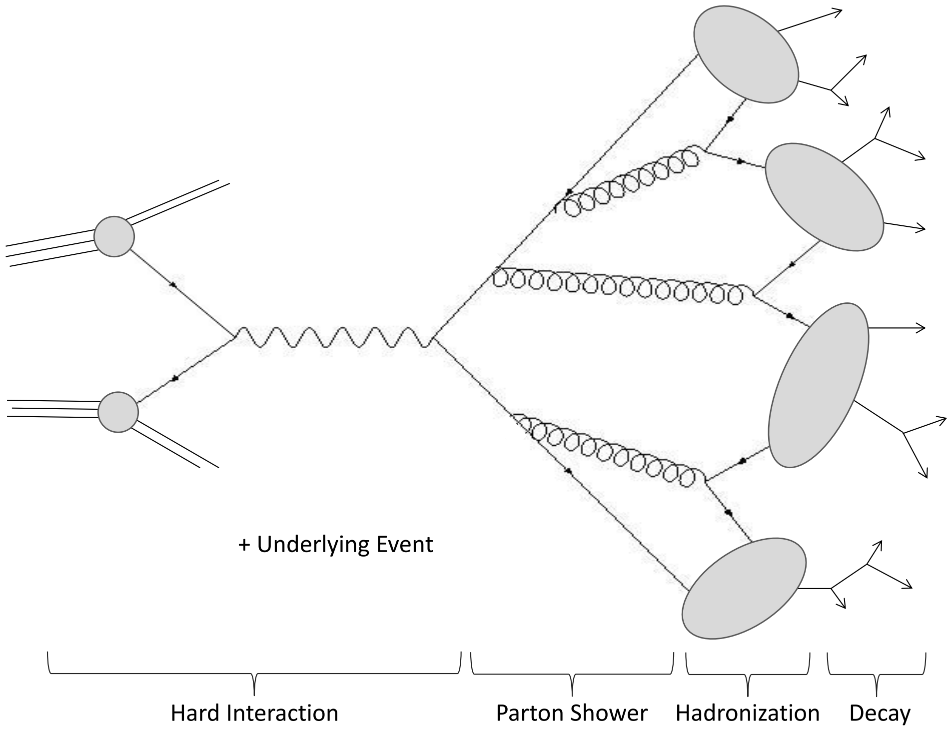

Figure 3.10: Sketch of individual steps in the generation process of simulated events.

collisions and introduces some event generators including different approaches for the simulation of the detector. A broader overview of event simulation and respective generators for LHC physics can be e.g. found in [37, 38].

The simulation of high energy collisions is a quite challenging task as each collision involves typically several hundreds of particles with momenta ranging over some orders of magnitude. Furthermore, the collisions being subject to quantum chromodynamics are only calculable within approximation schemes where also numerical methods do not provide solutions within a reasonable amount of time. Thus, event simulation is primarily utilizing *Monte Carlo* (MC) techniques which rely on the repeated sampling of random numbers, cf. e.g. [39]. For convenience events obtained from simulation are often denoted by the label 'MC' in this thesis.
Typically, the generation of an event follows several subsequent steps which are illustrated in Fig. 3.10 and described in the following:

Hard process: The first step in the simulation of collision events is the description of the nominal proton-proton interaction which is typically referred to as *hard process*. The proton itself is not a fundamental particle but exhibits an internal structure . The constituents of which a proton is made off are known as *partons*. Thus two protons interact when there is a momentum transfer Q taking place between two individual partons. The probability for individual partons to take part in the hard interaction is parametrized by the *parton-distribution functions* (PDFs) which have been determined experimentally . The value of x denotes the fraction of the

Quelle: Proton Struktur

Quelle:PDFs

longitudinal momentum carried by an individual parton. Consequently, the initial state of a proton-proton collision is not exactly known. Nevertheless, the cross section of a specific process can be calculated following the *factorization theorem* [40, 41]. Here, the hard interaction is described via perturbation theory and low-energy processes are considered in the phenomenological models of the respective PDFs. Thus the cross section for a process $ab \to n$ is given according to

$$\sigma = \sum_{a,b} \int_0^1 dx_a \, dx_b \int f_a(x_a, \mu_F) f_b(x_b, \mu_F) \, d\hat{\sigma}_{ab\to n}(\mu_F, \mu_R). \tag{3.6}$$

Here, $f(x, \mu_F)$ are the PDFs of the interacting protons which depend on the factorization scale μ_F whereas $\sigma_{ab\to n}$ indicates the parton-level cross section for the production of a final state n from partons a and b. This parton-level cross section depends on the final-state phase space, the factorization scale and the renormalisation scale μ_R as well as the corresponding matrix element. The factorization and renormalization scale are unphysical and have to be chosen for the generation process. Often the process possesses a typical hard scale Q^2 so that the choice $\mu_F = \mu_R = Q^2$ is made. However, this choice is not fixed by first principles.

Parton shower: After the production in the hard interaction the outgoing partons start to form a shower, i. e. cascades of further partons emerge. Typically, this happens with descending amounts of momentum transfer from the high scales down to low scales around 1 GeV. This evolution is typically described by a probabilistic shower algorithm. In addition to a parton shower related to the outgoing partons which is referred to as *final-state radiation* (FSR), partons can already radiate off other partons before the actual hard process takes place. This effect is known as *initial-state radiation* and can be described by similar principles as FSR. However, in the case of ISR it is inevitable to consider that not all partons from the ISR shower necessarily take part in any hard process and thus have to be related to the proton remnant.

Hadronization: The evolution of the parton shower continues until low scales in momentum transfer are reached and so the final state partons eventually start to form colour neutral hadrons. In the context of simulation the term *hadronization* describes the particular model which is used in order to specify the transition from the partonic state to the complete hadronic final state. Since the hadronization involves low-energetic processes it can not be treated within perturbation theory. In principle one distinguishes between *string models* (cf. e.g. [42]) and *cluster models* (cf. e.g. [43, 44]) in order to characterize the hadronization. While the first model describes directly the transition from the parton to the hadron based on the assumption of linear confinement, the second model introduces an intermediate step of cluster objects with mass scales around a few GeV. Particles arising from the hadronization are denoted with *generator-level* particles and labelled 'gen' within this thesis.

Decay: After the hadronization process a couple of unstable hadrons are present in the event whose decay into stable particles must be modelled. Stable in this context means that they do not decay further within the typical collider timescales. Thus, the observable final-state hadrons result from a convolution of the hadronization process with the decay modelling. Concerning the decay process a choice has to be made regarding the hadrons which shall be included in the simulation and the respective decay modes which have to be considered. Mainly, theses choices are based on experimental results in combination with theoretical assumptions. Typical differences occur e.g. in the consideration of excited mesons or heavy baryon multiplets as well as an appropiate treatment of matrix elements and spin correlations during the decay.

Underlying event: In addition to hadrons emerging from the process connected directly to the hard interaction, further contributions to the event can be present which is reffered to as *underlying event* (UE). The UE activity can be e.g. caused by additional interactions occuring for incoming partons, which is known as *multiple parton interaction* (MPI), or by interactions arising from the proton remnants. In general, such effects contribute to the total amount of scattered energy and increase the number of particles appearing in the hadronization process.

The various sub-processes described above are the basis of various event generators which differ in some aspects concerning the treatment of individual sub-processes in the event simulation. In this thesis, different generators are used:

PYTHIA [45]: Pythia is a general purpose event generator which has been used already extensively at previous collider experiments. It is designed to simulate collisions of either hadrons or same-generation leptons. This means that it is well suited to modell the required *pp* collisions, but is currently not usable for e.g. *ep* or γp processes. The highest multiplicity of particles involved in the hard interaction that can be simulated with Pythia are $2 \rightarrow 3$ processes. Nonetheless, more than three final state particles can arise for instance from the parton shower. Besides the simulation of whole physics events including all relevant steps, Pythia can also be interfaced to other generator programs in order to carry out the parton shower and hadronization step only.

HERWIG++ [46]: Herwig++ is as well as Pythia a general purpose MC generator. It provides the possibility to simulate high-energy collisions for lepton-lepton, lepton-hadron and hadron-hadron processes with special emphasis on the modelling of QCD radiation. Thus, the distinct feature of Herwig++ is that colour coherence effects are taken into account by employing angular ordered parton showers meaning that the coherence of soft radiation is treated correctly.

MADGRAPH [47]: Madgraph is a general-purpose matrix-element program and designed to provide accurate descriptions of multiparton processes. It can commonly be interfaced to Pythia for the realisation of the showering and hadronization.

POWHEG [48]: The powheg programme provides accurate QCD computations based on matrix elements up to next-to-leading order following the concept proposed in [49]. It can be interfaced to shower programs like Pythia or Herwig++ in order to perform the subsequent showering process.

In order to evaluate the interaction of the generated particles with the detector material the passage of the particles through the detector is simulated. This is done based on a detailled model of the CMS apparatus utilizing the GEANT4 programme [50] and referred to as *full simulation*. Full simulation is quite extensive in computing time and thus for several purposes also a simplified scheme of the detector model is used which is known as *fast simulation* [51]. Especially in analyses where many signal samples are needed to scan a wide parameter range, like e.g. in SUSY analyses, the usage of the fast simulation is very beneficial. A comparison of several relevant kinematic distributions in real collision events to simulated events obtained from fast simulation shows a quite good agreement [52]. In particular, also jet related quantities like the sum of calorimetric jet momenta or the missing transverse momentum are modelled with a similar accuracy in full and fast simulation. Finally, recorded collision data as well as simulated events including the modelling of the passage through the detector are present in the same data format which allows to apply equal reconstruction techniques in order to derive physics objects from the obtained events.

4 Object Reconstruction and Particle Identification

4.1 Global Event Description with the Particle-Flow Algorithm at CMS

4.2 Reconstruction of Jets

4.2.1 Jet Algorithms

4.2.2 Jet Types at CMS

4.2.3 Jet Energy Calibration

4.3 Identification of B-Hadron Decays

4.4 Identification of Boosted Top Quark Decays

4.4.1 The CMS Top Tagger

4.4.2 The HEP Top Tagger

4.4.3 Subjet B-Tagging

4.4.4 N-subjettiness

5 Measurement of the Jet Transverse-Momentum Resolution

5.1 Basic Concept of the Dijet Asymmetry Method

5.2 Apllication to Realistic Collision Events

5.3 Samples and Event Selection

5.3.1 Datasets and Triggers

5.3.2 Selection Criteria

5.4 Corrections to the Dijet Asymmetry

5.4.1 Correction for Additional Jet Activity

5.4.2 Correction for Particle-Level Imbalance

5.4.3 Results of the Corrections to the Asymmetry

5.5 Determination of the Data-to-Simulation Ratio of the Jet Transverse Momentum Resolution

5.6 Validation of the Method

5.6.1 Validation in Simulated Events

5.6.2 Validation of the Measured Data-to-Simulation Ratio

5.7 Systematic Uncertainties

5.8 Extension of the Method to the Forward Detector Region

5.9 Results

5.9.1 Comparison to Other Measurements

6 Search for New Physics in the Multijet and Missing Transverse Momentum Final State at $\sqrt{s} = 8$ TeV

6.1 Event Selection

6.1.1 Data samples and trigger

6.1.2 Event Cleaning

6.1.3 Baseline Selection

6.1.4 Exclusive Search Regions

6.2 QCD Background Estimation with the Rebalance-And-Smear Method

6.2.1 Rebalance Procedure using Kinematic Fits

6.2.2 Response Smearing

6.2.3 Validation Tests

6.2.4 Systematic Uncertainties

6.2.5 QCD Background Prediction

6.3 Estimation of Non-QCD Backgrounds

6.3.1 Invisible Z Background

6.3.2 Hadronic τ Background

6.3.3 Lost-Lepton Background

6.4 Results and Interpretation

6.4.1 Comparison to Other Measurements

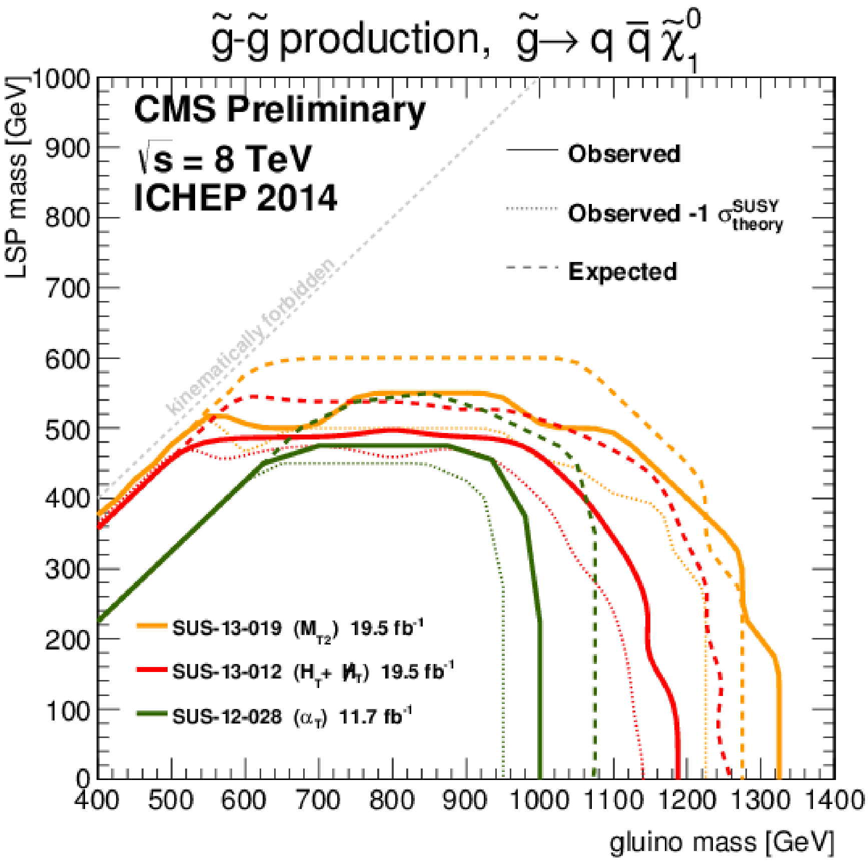

Figure 6.1: Comparison of various exclusion limits derived by different CMS anlayses for the SMS T1qqqq. Taken from ... (cms susy public results).

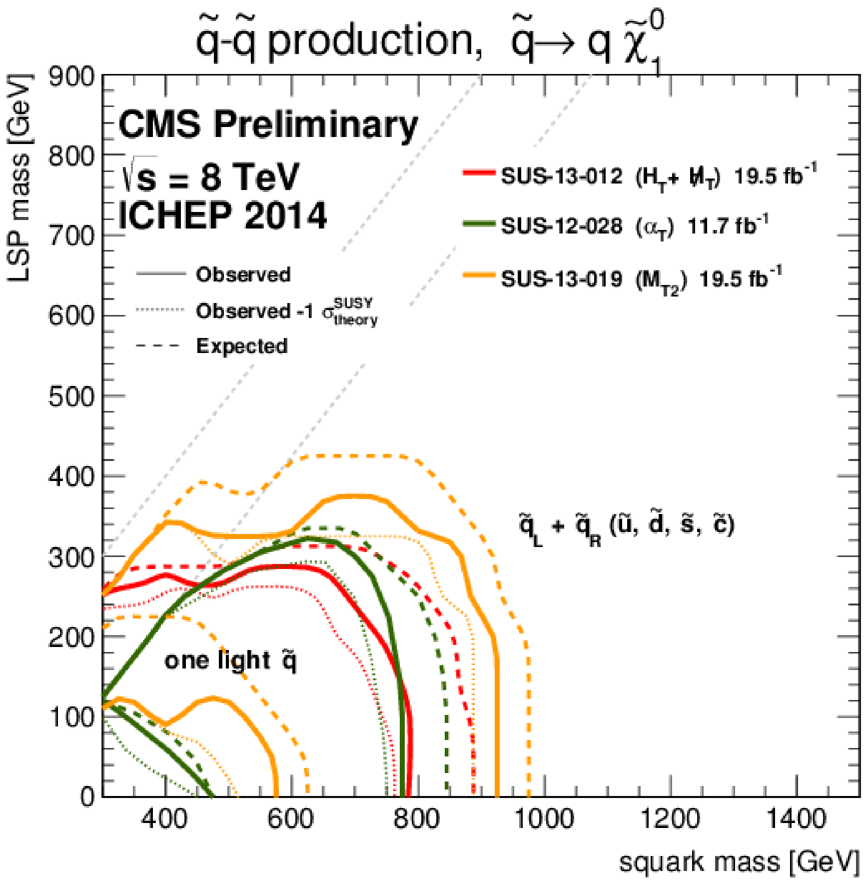

Figure 6.2: Comparison of various exclusion limits derived by different CMS anlayses for the SMS T2qq. Taken from ... (cms susy public results).

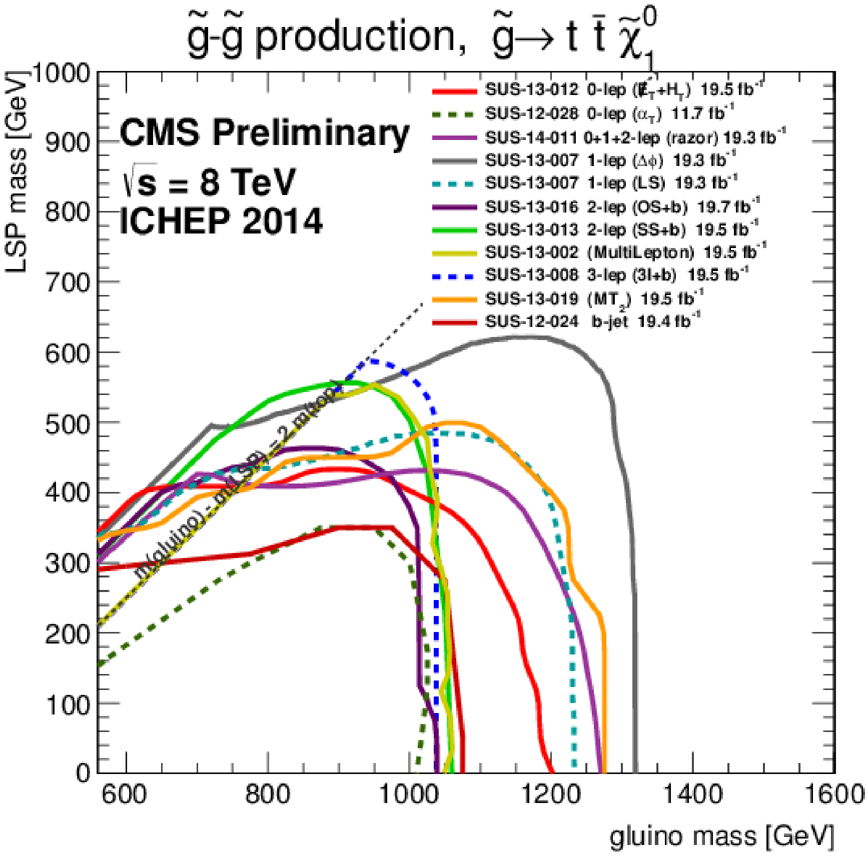

Figure 6.3: Comparison of various exclusion limits derived by different CMS anlayses for the SMS T1tttt. Taken from ... (cms susy public results).

7 Prospect Studies for a Search for Top Squarks in Events with Jets and Missing Transverse Momentum at $\sqrt{s} = 13$ TeV

7.1 Data samples

7.2 Top Tagging Efficiency Studies

7.2.1 Top Tag Efficiency

7.2.2 Misidentification Rate

7.3 Studies towards a Suitable Analysis Strategy

7.4 Results and Discussion

7.4.1 Comparison of the Performance of Various Selections

7.4.2 Discussion of Specific Simplified Assumptions in the Analysis

8 Conclusions

Supersymmetry is among the favoured extensions of the standard model of particle physics and one of the main target of searches for new physics within the CMS experiment. Since especially coloured SUSY particles are expected at a high rate at the LHC which predominantly manifest in final states containing jets and missing transverse momentum, it is promising to perform searches based on such signatures which require in addition a good understanding of jet properties.

In this thesis, a measurement of the jet transverse momentum resolution in dijet events corresponding to data with an integrated luminosity of 19.8 fb^{-1} recorded at $\sqrt{s} = 8$ TeV in 2012 by the CMS experiment has been presented. A similar approach to previous analyses was used, but the precision of the measurement could be significantly improved. This was achieved by a correct treatment of statistical uncertainties by considering correlations among inclusive distributions which subsequently also allowed a revised treatment of systematic uncertainties which have been conservatively overestimated in the past. Furthermore, the method has been extended to be able to measure the resolution in the forward part of the detector with higher precision. For $|\eta| = 0.0 - 5.0$ the data-to-simulation ratio of the resolution has been measured. Since no significant trend as function of $p_{\mathrm{T}}^{\mathrm{ave}}$ was apparent, the ratio is determined as function of $|\eta|$ only. The ratios obtained for the various $|\eta|$ regions increase from 1.079 ± 0.026 in the central region up to 1.395 ± 0.063 at $|\eta| = 2.8 - 3.2$ and drop again for the outermost region $|\eta| = 3.2 - 5.0$ down to 1.056 ± 0.191. These values can be utilized to adjust the resolution in simulation to match the one observed in data.

In the second part of this thesis, a search for supersymmetry in events with $N_{\mathrm{Jets}} = 3-5, 6-7, \geq 8$ and large missing momentum in proton-proton collsions at $\sqrt{s} = 8$ TeV in data corresponding to an integrated luminosity of 19.5 fb^{-1} has been presented. Special emphasis is put on the determination of the QCD multijet background which relies strongly on the precise knowledge of the jet response. These QCD background contributions are estimated directly from multijet events in data by modelling momentum mismeasurements based on the jet response. A similar approach has been used already in earlier versions of this analysis where the search has been performed inclusive in the jet multiplicity requiring at least three jets. With the extension of the analysis to multijet events, an adjustment of the method to predict QCD multijet background contributions became inevitable. A dedicated correction to the existing method has been introduced in order to predict the jet multiplicity correctly. Moreover the assignment of systematic uncertainties has been revised in order to consider e.g. the challenging conditions due to pile-up appropriately. In total, the QCD multijet background could be estimated with a precision of approximately $70 - 80\%$ in search regions with non-negligible QCD background contributions. The observed number of events in data are consistent with the expected number of events from standard model processes such that exclusion limits are derived for various simplified supersymmetric models. In the context of this simplified models the production of squarks below 780 GeV and that of gluinos up to $1.1 - 1.2$ TeV can be excluded at 95% CL for

LSP masses not exceeding 100 GeV.
In addition to inclusive searches targeting gluinos and squarks, CMS has also peformed searches for direct production of top squarks with data obtained at $\sqrt{s} = 8$ TeV. With this data direct poduction of top squarksdecaying into top and LSP could be excluded up to top squarks masses of approximately 750 GeV for LSP masses below 100 GeV. In order to extend the mass reach of such searches to even higher top squark masses in the next run period of the LHC which will start in 2015 with a center of mass energy of 13 TeV suitable selection criteria for such analyses have been investigated in the third part of this thesis. Studies presented here are based on events with several jets, large momentum imbalance and no leptons. One key aspect is the application of dedicated algorithms for the identification of decay products emerging from boosted top decays in order to separate possible SUSY signal events from standard model background. Various different discriminating variables have been investigated. Moreover the sensitivity of several selections – also that one of the all-hadronic stop search performed at $\sqrt{s} = 8$ TeV– has been compared by deriving the expected exclusion reach for data corresponding to 19.5 fb^{-1} at $\sqrt{s} = 13$ TeV. Selection criteria could be identified extending the mass reach of direct stop searches up to roughly 1 TeV for LSP masses below 100 GeV.

Summary in den Kontext "Natural SUSY" einbetten

Bibliography

[1] J. B. et al. (Particle Data Group)), "Review of Particle Physics", *Phys. Rev. D* **86** (Jul, 2012) 010001. `doi:10.1103/PhysRevD.86.010001`.

[2] N. Cabibbo, "Unitary Symmetry and Leptonic Decays", *Phys. Rev. Lett.* **10** (Jun, 1963) 531 – 533. `doi:10.1103/PhysRevLett.10.531`.

[3] M. Kobayashi and T. Maskawa, "CP-Violation in the Renormalizable Theory of Weak Interaction", *Progress of Theoretical Physics* **49** (1973), no. 2, 652–657. `doi:10.1143/PTP.49.652`.

[4] R. Alkofer and J. Greensite, "Quark Confinement: The Hard Problem of Hadron Physics", *J.Phys.* **G34** (2007) S3, `arXiv:hep-ph/0610365`. `doi:10.1088/0954-3899/34/7/S02`.

[5] H. D. Politzer, "Reliable Perturbative Results for Strong Interactions?", *Phys. Rev. Lett.* **30** (Jun, 1973) 1346 – 1349. `doi:10.1103/PhysRevLett.30.1346`.

[6] D. J. Gross and F. Wilczek, "Ultraviolet Behavior of Non-Abelian Gauge Theories", *Phys. Rev. Lett.* **30** (Jun, 1973) 1343 – 1346. `doi:10.1103/PhysRevLett.30.1343`.

[7] S. Glashow, "Partial Symmetries of Weak Interactions", *Nucl.Phys.* **22** (1961) 579–588. `doi:10.1016/0029-5582(61)90469-2`.

[8] S. Weinberg, "A Model of Leptons", *Phys.Rev.Lett.* **19** (1967) 1264–1266. `doi:10.1103/PhysRevLett.19.1264`.

[9] P. W. Higgs, "Broken Symmetries and the Masses of Gauge Bosons", *Phys. Rev. Lett.* **13** (1964) 508 – 509. `doi:10.1103/PhysRevLett.13.508`.

[10] F. Englert and R. Brout, "Broken Symmetry and the Mass of Gauge Vector Mesons", *Phys. Rev. Lett.* **13** (1964) 321 – 323. `doi:10.1103/PhysRevLett.13.321`.

[11] G. S. Guralnik, C. R. Hagen, and T. W. B. Kibble, "Global Conservation Laws and Massless Particles", *Phys. Rev. Lett.* **13** (1964) 585 – 587. `doi:10.1103/PhysRevLett.13.585`.

[12] ATLAS Collaboration Collaboration, "Observation of a new particle in the search for the Standard Model Higgs boson with the ATLAS detector at the LHC", *Phys.Lett.* **B716** (2012) 1–29, `arXiv:1207.7214`. `doi:10.1016/j.physletb.2012.08.020`.

[13] CMS Collaboration Collaboration, "Observation of a new boson at a mass of 125 GeV with the CMS experiment at the LHC", *Phys.Lett.* **B716** (2012) 30–61, `arXiv:1207.7235`. `doi:10.1016/j.physletb.2012.08.021`.

[14] ATLAS Collaboration Collaboration, "Measurements of Higgs boson production and couplings in diboson final states with the ATLAS detector at the LHC", *Phys.Lett.* **B726** (2013) 88–119, `arXiv:1307.1427`. `doi:10.1016/j.physletb.2013.08.010`.

[15] ATLAS Collaboration Collaboration, "Measurements of Higgs boson production and couplings in the four-lepton channel in pp collisions at center-of-mass energies of 7 and 8 TeV with the ATLAS detector", `arXiv:1408.5191`.

[16] ATLAS Collaboration Collaboration, "Measurement of Higgs boson production in the diphoton decay channel in *pp* collisions at center-of-mass energies of 7 and 8 TeV with the ATLAS detector", `arXiv:1408.7084`.

[17] CMS Collaboration Collaboration, "Precise determination of the mass of the Higgs boson and studies of the compatibility of its couplings with the standard model", Technical Report CMS-PAS-HIG-14-009, CERN, Geneva, 2014.

[18] M. Beyer, ed., "CP Violation in Particle, Nuclear, and Astrophysics". Lecture Notes in Physics. Springer, 2010. ISBN 3-642-07830-3.

[19] Planck Collaboration Collaboration, "Planck 2013 results. XVI. Cosmological parameters", *Astron.Astrophys.* (2014) `arXiv:1303.5076`. `doi:10.1051/0004-6361/201321591`.

[20] G. Bertone, D. Hooper, and J. Silk, "Particle dark matter: Evidence, candidates and constraints", *Phys.Rept.* **405** (2005) 279–390, `arXiv:hep-ph/0404175`. `doi:10.1016/j.physrep.2004.08.031`.

[21] I. J. Aitchison, "Supersymmetry and the MSSM: An Elementary introduction", `arXiv:hep-ph/0505105`.

[22] S. P. Martin, "A Supersymmetry primer", *Adv.Ser.Direct.High Energy Phys.* **21** (2010) 1–153, `arXiv:hep-ph/9709356`.

[23] O. S. Brüning, P. Collier, P. Lebrun et al., "LHC Design Report", volume 1: The LHC Main Ring. CERN, Geneva, 2004. CERN-2004-003-V-1.

[24] L. Evans and P. Bryant, "LHC Machine", *Journal of Instrumentation* **3** (2008), no. 08, S08001. `doi:10.1088/1748-0221/3/08/S08001`.

[25] CERN, "LEP Design Report", volume 2: The LEP Main Ring. CERN, Geneva, 1984. CERN-LEP-84-01.

[26] CERN, "LHC: the guide (English version)". CERN-Brochure-2009-003-Eng, 2009.

[27] 2012. W.J. Stirling, private communication.

[28] ATLAS Collaboration, "The ATLAS Experiment at the CERN Large Hadron Collider", *JINST* **3** (2008) S08003. `doi:10.1088/1748-0221/3/08/S08003`.

[29] CMS Collaboration, "The CMS experiment at the CERN LHC", *JINST* **3** (2008) S08004. `doi:10.1088/1748-0221/3/08/S08004`.

[30] CMS Collaboration, "CMS Detector Performance and Software", volume 1 of *CMS Physics Technical Design Report*. CERN, Geneva, 2006. CMS-TDR-008-1. CERN-LHCC-2006-001.

[31] LHCb Collaboration, "The LHCb Detector at the LHC", *JINST* **3** (2008) S08005. `doi:10.1088/1748-0221/3/08/S08005`.

[32] ALICE Collaboration, "The ALICE experiment at the CERN LHC", *JINST* **3** (2008) S08002. `doi:10.1088/1748-0221/3/08/S08002`.

[33] CMS Collaboration, "The CMS tracker system project", volume 5 of *Technical Design Report CMS*. CERN, Geneva, 1997. CMS-TDR-005. CERN-LHCC-98-006.

[34] CMS Collaboration, "Luminosity Information for the 2012 Proton Run", 2012. `https://twiki.cern.ch/twiki/bin/view/CMSPublic/LumiPublicResults`.

[35] "LHC machine outreach", 2013. `http://lhc-machine-outreach.web.cern.ch/lhc-machine-outreach/`.

[36] M. Lamont, "Status of the LHC", *J.Phys.Conf.Ser.* **455** (2013) 012001. `doi:10.1088/1742-6596/455/1/012001`.

[37] M. H. Seymour and M. Marx, "Monte Carlo Event Generators", `arXiv:1304.6677`.

[38] A. Buckley, J. Butterworth, S. Gieseke et al., "General-purpose event generators for LHC physics", *Phys.Rept.* **504** (2011) 145–233, `arXiv:1101.2599`. `doi:10.1016/j.physrep.2011.03.005`.

[39] N. Metropolis and S. Ulam, "The Monte Carlo Method", *Journal of the American Statistical Association* **44** (1949), no. 247, 335–341. `doi:10.2307/2280232`.

[40] J. C. Collins and D. E. Soper, "The Theorems of Perturbative QCD", *Ann.Rev.Nucl.Part.Sci.* **37** (1987) 383–409. `doi:10.1146/annurev.ns.37.120187.002123`.

[41] J. C. Collins, D. E. Soper, and G. F. Sterman, "Factorization of Hard Processes in QCD", *Adv.Ser.Direct.High Energy Phys.* **5** (1988) 1–91, `arXiv:hep-ph/0409313`.

[42] B. Andersson, G. Gustafson, G. Ingelman et al., "Parton fragmentation and string dynamics", *Physics Reports* **97** (1983), no. 2 - 3, 31 – 145. `doi:http://dx.doi.org/10.1016/0370-1573(83)90080-7`.

[43] D. Amati and G. Veneziano, "Preconfinement as a property of perturbative QCD", *Physics Letters B* **83** (1979), no. 1, 87 – 92. `doi:http://dx.doi.org/10.1016/0370-2693(79)90896-7`.

[44] A. Bassetto, M. Ciafaloni, and G. Marchesini, "Color singlet distributions and mass damping in perturbative QCD", *Physics Letters B* **83** (1979), no. 2, 207 – 212. `doi:http://dx.doi.org/10.1016/0370-2693(79)90687-7`.

[45] T. Sjostrand, S. Mrenna, and P. Z. Skands, "PYTHIA 6.4 Physics and Manual", *JHEP* **0605** (2006) 026, `arXiv:hep-ph/0603175`. `doi:10.1088/1126-6708/2006/05/026`.

[46] M. Bahr, S. Gieseke, M. Gigg et al., "Herwig++ Physics and Manual", *Eur.Phys.J.* **C58** (2008) 639–707, `arXiv:0803.0883`. `doi:10.1140/epjc/s10052-008-0798-9`.

[47] J. Alwall, R. Frederix, S. Frixione et al., "The automated computation of tree-level and next-to-leading order differential cross sections, and their matching to parton shower simulations", *JHEP* **1407** (2014) 079, `arXiv:1405.0301`. `doi:10.1007/JHEP07(2014)079`.

[48] C. Oleari, "The POWHEG-BOX", *Nucl.Phys.Proc.Suppl.* **205-206** (2010) 36–41, `arXiv:1007.3893`. `doi:10.1016/j.nuclphysbps.2010.08.016`.

[49] P. Nason, "A New method for combining NLO QCD with shower Monte Carlo algorithms", *JHEP* **0411** (2004) 040, `arXiv:hep-ph/0409146`. `doi:10.1088/1126-6708/2004/11/040`.

[50] S. Agostinelli, J. Allison, K. Amako et al., "G4 – a simulation toolkit", *Nuclear Instruments and Methods in Physics Research Section A: Accelerators, Spectrometers, Detectors and Associated Equipment* **506** (2003), no. 3, 250 – 303. `doi:10.1016/S0168-9002(03)01368-8`.

[51] CMS Collaboration Collaboration, "The fast simulation of the CMS detector at LHC", *J.Phys.Conf.Ser.* **331** (2011) 032049. `doi:10.1088/1742-6596/331/3/032049`.

[52] CMS Collaboration Collaboration, "Comparison of the Fast Simulation of CMS with the first LHC data",. CMS-DP-2010-039.